Acousto-optical radio-wave spectrometer with parallel multi-channel data processing for astrophysical investigations

Technical Report No. 634

Principal contributors:

Alexandre S. Shcherbakov, Miguel Chavez Dagostino, Adán Omar Arellanes, and Arturo Aguirre López.

National Institute for Astrophysics, Optics, and Electronics (INAOE), Puebla, Mexico.

National Institute for Astrophysics, Optics, and Electronics (INAOE),

Puebla, Mexico.

Department for Optics, INAOE

Index

ABSTRACT.

We develop a multi-band spectrometer with a few spatially parallel optical arms for the combined processing of their data flow. Such multi-band capability has various applications in astrophysical scenarios at different scales: from objects in the distant universe to planetary atmospheres in the Solar system. Each optical arm exhibits original performances to provide parallel multi-band observations with different scales simultaneously. Similar possibility is based on designing each optical arm individually via exploiting different materials for acousto-optical cells operating within various regimes, frequency ranges and light wavelengths from independent light sources. Individual beam shapers provide both the needed incident light polarization and the required apodization to increase the dynamic range of a system. After parallel acousto-optical processing, data flows are united by the joint CCD matrix on the stage of the combined electronic data processing. At the moment, the prototype combines still three bands, i.e. includes three spatial optical arms. The first low-frequency arm operates at the central frequencies ~60-80 MHz with frequency bandwidth ~40 MHz. The second arm is oriented to middle-frequencies ~350-500 MHz with frequency bandwidth ~200-300 MHz. The third arm is intended for ultra-high-frequency radio-wave signals about 1.0-1.5 GHz with frequency bandwidth >300 MHz. To-day, this spectrometer has the following preliminary performances. The first arm exhibits frequency resolution ~20 KHz; while the second and third arms give the resolution ~150-200 KHz. The numbers of resolvable spots are 1500-2000 depending on the regime of operation. The fourth optical arm at the frequency range ~3.5 GHz is currently under construction.

Keywords: Acousto-optics, Spectroscopy, Radio-wave astrophysics

1 INTRODUCTION

During the last years a lot of novelties related to using the acousto-optics (AO) to various physical applications, in particular to spectrum analysis radio-wave and optical signals had been developed. For example, theoretical analysis had been developed with relativistic considerations and rigorous coupled wave analysis had been generalized for the diffraction within the AO effect [1]. Also, there are applications in fiber optics, where the AO effect is exploited to shape the transmission spectrum [2], and it had been demonstrated recently that the AO effect can be applied to generate Bessel beams with liquid AO arrays [3]. The spectroscopic capabilities of the AO devices had been in continuous improvement up to these days for several kinds of spectroscopic needs; from astrophysics [4-6] to biomedics [7-9]. Broadly speaking, the AO spectrometers can work in two ways: the first one is the analysis of optical signals (from UV to IR) utilizing UHF signals inserted to the piezoelectric-transducer of the AO cell; the second one is the analysis of radio-wave signals directly introduced to the piezoelectric-transducer and study the diffraction of a laser occurred due to this radio-wave signal. We are considering the second option for its use in radio-astronomy in 3 different bands.

In section 2 we describe our proposal for implementing the three AO spectrometers describing the benefits of the device and the problems we are addressing. In section 3 we depict the potential performance that is expected from our device, namely, its bandwidth, efficiency, and resolution for the three materials we are considering. In section 4 we analyze the apodization of signals to improve the performance of the device. In section 5, we show the experimental data for one of the bands discussed in previous sections to corroborate our theoretical estimations. In section 6, we discuss the conclusions of our present research.

2. GENERAL CONSIDERATION

Within this article, a pioneer approach to designing a prototype of the acousto-optic (AO) spectrometer for radio-astronomy is schematically analyzed as well as preliminary confirmed by both the practical estimations and proof-of-principal experiments. The advances under this proposal reflect the next step in a progress in this field that includes principally higher level of parallelism in a wideband analogue signal processing with various frequency performances simultaneously and selecting the most appropriate AO materials for the desirable algorithm of processing. As it had been described recently [6], any prototype of AO radio-wave spectrometer is based on injecting ultra-high-frequency (UHF) radio-signals into a large-aperture AO cell via effective piezoelectric transducer. Similar signals give birth to a large amount of dynamic acoustic gratings (each corresponds to a partial frequency from the initial UHF radio-signal), which modulate the incident widely expanded light beam of a fixed wavelength. In so doing, the incident monochromatic light beam is divided into sets of the partial light beams originating independent parallel frequency channels and being scanned at the angles depending on the partial acoustic frequencies. Then, the intensities of partial light beams are determined by the amplitudes of partial frequency components inherent in the initial UHF radio-signal. Later, these partial light beams are focused by the Fourier-transforming lens system on a CCD-array for the further computer processing.

The principal difference of the schematic arrangement under presentation in comparison with the previously described one [6], consists in the fact that now we develop the scheme with a few of almost independent spatially parallel arms for data processing. Now, each individual spatial arm exhibits its own original performances to provide a parallel observation of astrophysical objects within a few different scales simultaneously. Similar possibility is based on designing each of these spatial arms perfectly individually with exploiting different materials for AO cells operating within different regimes at different frequency ranges and light wavelengths from completely independent sources of coherent light. Moreover, these spatial arms have now the beam shapers providing both the needed states of the incident light beam polarization in each arm and the required apodization for the incident light beams to suppress side lobes in the Fourier-transform plane, i.e. to increase the dynamic range of total processing system. Finally, after AO processing, all these data flow are united by the joint matrix CCD photo-detector already on the stage of a high-bit-rate electronic data processing. At the moment, we have restricted ourselves by only the three similar spatial arms for data processing and for simplicity sake only one spatial arm of this three-arm schematic arrangement is shown in Fig.1 in detail. The first spatial arm of data processing represents almost a replica of the optoelectronic scheme described previously [6], so that it need not a lot of additional comments. Nevertheless, now it uses now the single frequency solid-state laser CL-442-025-S (CrystaLaser) at optical wavelength λ = 442 nm to decrease the spot size d due to $d \propto \lambda$. It is based on a low frequency and extremely effective tellurium dioxide AOC with the central frequency of analysis close to 60 – 80 MHz and the frequency bandwidth below 100 MHz. The second arm is oriented to the spectrum analysis of let say middle-frequency radio-wave signals with the central frequencies belonging to a range bordered on 350 – 500 MHz and the frequency bandwidth about 100 – 300 MHz. This spatial arm can exploit the AO cells

based on such effective single crystals as gallium phosphide (GaP) or z-tellurium dioxide ($z–TeO_2$) crystals operating in the regime of normal light scattering in the visible range of spectrum. The third arm of processing is intended for direct spectrum analysis of UHF radio-signals whose the central frequencies exceed 1.5 GHz and the frequency bandwidth are over 300 MHz. At the moment, the third spatial arm oriented to an AO cell based on rather specific cut of a lithium niobate ($LiNbO_3$) crystal providing the anomalous regime of light scattering in the near infrared optical range. Potentially, one can already have imagined the fourth spatial arm directed to reaching the frequency bandwidths over 1 GHz with the corresponding growth of the central frequencies. The most adequate approaches for realizing similar bandwidths practically can be based on either the phased-array technique [10] or the technique [11] for the piezoelectric transducer design.

Each the enumerated spatial arm for spectrum analysis within the prototype under discussion consists of a few optical or optoelectronic sub-systems, namely:
a) rather powerful coherent light source controlling the linear polarization state and operating in a single frequency regime with small (about 1 – 3 mrad) beam divergence;
b) beam shaper providing the desirable degree of linear polarization as well as the needed expansion and apodization of that beam;
c) AO ell represents by itself specifically operating opto-electronic sub-systems, which determine the main performances of taken spatial arm,
d) Fourier-transform system including the integrating lens with an individual row of the CCD-matrix, see Fig.1.

The three AO cells are key components of a new spectrometer under consideration, because just these components determine the efficiency of operation, the frequency bandwidth of spectrum analysis, and the frequency resolution, i.e. the accuracy of radio-wave signals identification. The criteria of selecting the concrete material can depend on various requirements such as high light diffraction efficiency or a large angle of light beam deflection, or just minimal acoustic wave attenuation to achieve as high as possible operation frequencies, and so on. Together with this, even an individual spatially one-channel AO cell provides a multi-channel (a thousand channels or more) parallel processing in the frequency domain in such a way that practical frequency range of AO cell's operation can be varied in wide limits to be perfectly adequate to the observational needs of modern radio-astronomy. These needs are widely varied from the frequency bandwidth $\Delta f \approx$ 40 MHz and the frequency resolution $\delta f \geq$ 15 KHz to $\Delta f \approx$ 300 MHz and $\delta f \geq$ 100 KHz with the number of parallel processing channels in the frequency domain (or, what is the same, the number of resolvable spots) $N \approx (2 – 3) \times 10^3$ as the case requires. These performances can be achieved at the top of modern technology exploiting specially designed AO cells based on specifically selected crystalline materials and regimes of their operations as it has been noted above.

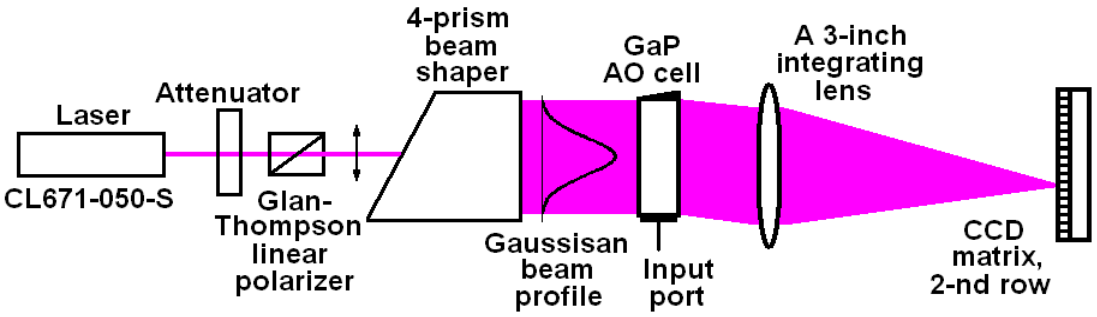

Figure 1. The second spatial arm for a new prototype of the acousto-optic spectrometer (vertical view).

At the current stage of development, our main goals assume the creation and sequential characterization of the enumerated sub-systems for the second arm with the wide-aperture AO cell based a GaP single crystal. This cell works at optical wavelength λ = 671 nm, which combines the convenience of operating in just the visible range with good enough transparency of this material with dark red light, from the single frequency solid-state laser CL-671-050-S (CrystaLaser). The GaP-cell is able to manage the radio-wave signals whose the best performances can be estimated as the central frequency is about 500 MHz, frequency bandwidth is close 250 MHz and frequency resolution about 105 KHz providing the number $N \approx 2 \times 10^3$ of resolvable spots or, what is the same, the number of parallel frequency channels for spectral data processing.

During the characterization of the beam shaper, including optical attenuator, linear polarization controller, and a four-prism beam expander, capable of apodizing that beam by the variable Gaussian profile, rather accurate adjusting the incident light beam had been achieved. The processing part of this spatial arm consists of a triplet of the following basic components. The first of them is represented by the above-mentioned gallium phosphide AO cell (Molecular Technology GmbH) with a 60 × 2 mm active optical aperture. The second component is a fragment of the 3-inch achromatic doublet lens (Edmund Optics) with the focal length of about 85 cm, while the third one is the second row of a 3-row CCD-matrix consisting of 3000 pixels of 7 μm × 200 μm each. The produced characterization shows that the main lobe of each partial optical beam can give the spot size of about 14-21 μm, so that it is lighting exactly two or three pixels of the CCD-row that guarantees optimal resolution of a pattern from viewpoint of the sampling theorem. General optical scheme of the second, i.e. the middle-frequency spatial arm for a new prototype of the AO spectrometer is presented in Fig.1.

3. POTENTIAL PERFORMANCES OF THE AO CELLS OPERATING WITHIN THE NORMAL LIGHT SCATTERING REGIME

3.1. Efficiency of light scattering with a given frequency bandwidth

AO interaction leads to deflection of the incident light beam by some angle that is directly proportional to frequency of the applied electric and, consequently, acoustic signal. One of the most important parameters for an AO cell, included into the Fourier processing, is the number of resolvable spots N in the image plane, which corresponds to the number of resolvable frequencies in the Fourier-transform plane. The number N can be determined as a ratio of the maximal light beam deflection angle $\Delta\theta$ to the beam divergence $\delta\theta \approx \lambda/D$ (with $n \approx 1$ in an air), where D is the linear size of that beam, i.e. $N = \Delta\theta\, D / \lambda$. The above-noted proportionality inherent in the Fourier transform makes it possible to explain $\Delta\theta = \lambda\, \Delta f / V$ in terms of the frequency bandwidth Δf and acoustic wave velocity V. Then, due to the transition time of passing an acoustic wave through AOC with an aperture coinciding with D is $\tau = D/V$, one can write

$$N = \tau \cdot \Delta f \ . \tag{1}$$

It is seen from Eq.(1) that if both the AO cell's-aperture D and consequently, the transition time τ are fixed, growing the number N can be provided only by increasing the bandwidth Δf. In so doing, the highest efficiency of light scattering is extremely desirable of course. However, the scattered light intensity depends on the angular-frequency mismatch η as well, which is conditioned by a wide range of varying the wave vectors of acoustic waves. Figure 2 represents the dependencies of the maximum scattered light intensity on the squared acoustic power parameter $\sigma \approx \pi\, \lambda^{-1}\, (P\, M^2/2)^{1/2}$, which combines contributions of the material properties and the acoustic power (M_2 is the figure of AO merit, P is the acoustic power density). The corresponding plots are shown for a triplet of the relative frequency bandwidths $\Delta f / f_0$ = 0, 0.25, and 0.5, where f_0 is the central acoustic frequency within the bandwidth Δf [12]. One can see that the efficiencies about 50% are approximately the same for all the taken values of the relative frequency bandwidth when $\sigma^2 \approx \pi/4$. By this it means that the maximum scattered light intensity will be almost the same for every frequency component under analysis with $\sigma^2 \approx \pi/4$ or, in the other words, the magnitude $\sigma^2 \approx \pi/4$ provides minimal variations of the scattered light intensity versus the applied frequency of a signal within the bandwidth Δf at the cost of decreasing the interaction efficiency by about 50%.

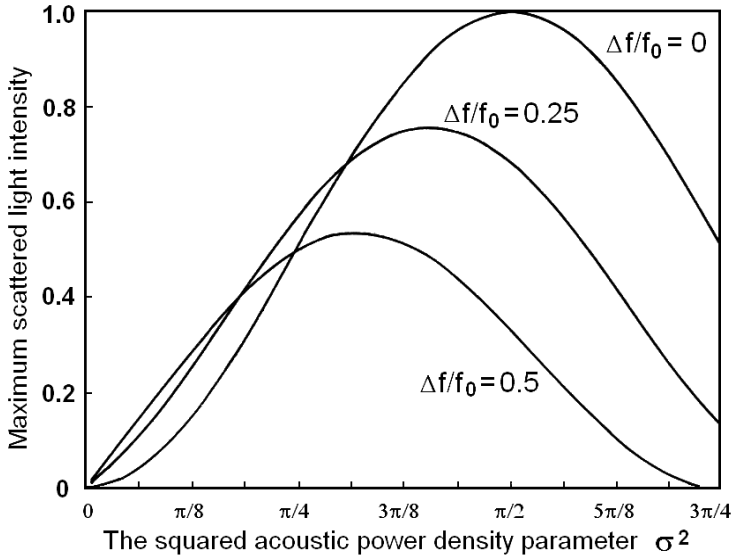

Figure 2. Maximal efficiency vs. the squared acoustic power density parameter $\sigma^2 \propto P$ and the relative frequency bandwidth $\Delta f / f_0$ [12].

3.2. The expected number of resolvable spots

The above-mentioned number of resolvable spots N characterizes either the number of frequency channels for parallel analysis or the frequency resolution inherent in processing optical system. The frequency bandwidth Δf of each AO cell depends on the chosen regime of light scattering. In the case of normal regime associated with a one-fold non-collinear light scattering, one can assume that the angle θ_0 of light incidence is rather small, so that $\cos \theta_0 \approx 1$, and the frequency bandwidth of a one-fold light can be expressed as $\Delta f = 2\, n\, V^2 / (\lambda\, L\, f_0)$. When the acoustic power density P is not too high and acoustic wave attenuation can be characterized as a moderate one, the frequency resolution of AO cell is determined by the formula $\delta f \approx V/D$ [13]. Thus, the number of resolvable spots can be expressed as $N = \Delta f / \delta f = 2\, n\, V\, D / (\lambda\, L\, f_0)$. Now, one can analyze a few factors limiting the number of resolvable spots as a function of the frequency parameters [12], and the main attention will be paid to similar dependence on the frequency bandwidth Δf. For this purpose, one can use the above-motivated preferable option $\Delta f \approx f_0/2$. Then, one can use the recently described approach to estimating the number N of resolvable spots, restricted by at least three physically independent limitations conditioned by aperture, geometry, and acoustic attenuation, see [6], section 6. Now, however, a one-phonon normal non-collinear light scattering is estimated for two other effective and available crystalline materials with $\Gamma \leq$ 10 [dB/(cm GHz^2)]**.**

3.2.1. Tellurium dioxide crystal (TeO_2)

Within a one-phonon light scattering in tellurium dioxide crystal, one can choose the normal process of AO interaction when the longitudinal elastic mode produces the acoustic beam along the [001] axis of that crystal. In this case, the following values: $V = 4.2 \times 10^5$ cm/s, λ = 633 nm, n = 2.26, and Γ = 10 dB/(cm GHz^2) are inherent in a so-called z-TeO_2 crystal. The needed numerical estimations have been done for the optical apertures D = 4, 5, 6, 7 cm; the attenuation factors along the full aperture B = 4, 5, 6 dB/aperture, and the

Klein-Cook parameter $Q = 3\pi, 4\pi$. One can see in Fig.3 that, for example, a tellurium dioxide AO cell with $D = 4$ cm, $Q > 3\pi$, and $B = 4$ dB/aperture is capable to provide $N \approx 1500$ resolvable spots at $f_0 \approx 320$ MHz, while with $D = 5$ cm, $Q > 4\pi$, and $B = 6$ dB/aperture the same cell is capable to provide $N \approx 2000$ resolvable spots at $f_0 \approx 350$ MHz.

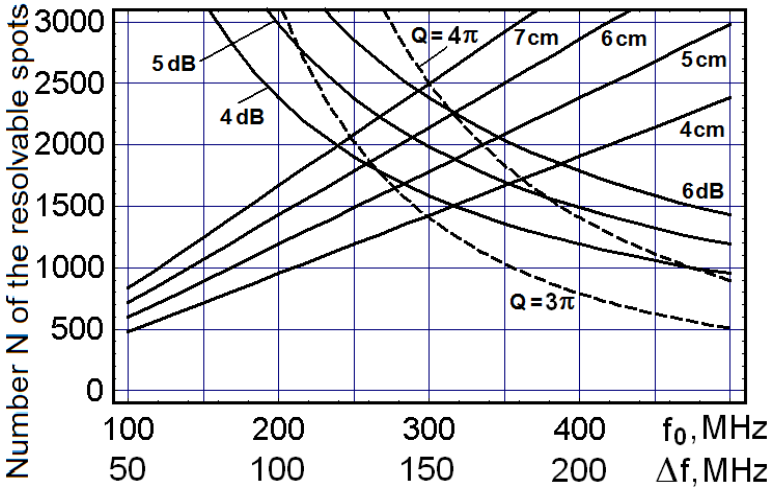

Figure 3. The combined diagram illustrating effect of a triplet of the restricting factors in a z–TeO_2 AO cell. The solid slowly growing lines are related to N_1, the chosen apertures D are equal to 4, 5, 6, and 7 cm. The dashed line regards to N_2 in the case of $Q = 3\pi$ and 4π. The solid hyperbolic-like falling curves illustrate N_3 and reflect contributions of the acoustic attenuation; the attenuation factors B are equal to 4, 5, and 6 dB along the aperture.

3.2.2. Gallium Phosphide (GaP)

The case of GaP-crystal is connected with the normal process when the longitudinal elastic mode produces the acoustic beam along the [110] axis, so that the following values inherent in this crystalline material: $V = 6.32 \times 10^5$ cm/s, $\lambda = 671$ nm, $n = 3.31$, and $\Gamma = 6$ dB/(cm GHz^2). The needed numerical estimations have been found for the apertures $D = 4, 5, 6, 7$ cm; the attenuation factors along the full aperture $B = 4, 5, 6, 7$ dB/aperture, and the Klein-Cook parameter $Q = 3\pi, 4\pi$, see Fig.4.

One can see that, for example, a gallium phosphide AO cell with $D = 5$ cm, $Q \approx 2\pi$, and $B \approx 4.5$ dB/aperture is capable to provide $N \approx 1500$ resolvable spots at $f_0 \approx 400$ MHz, while with $D = 7$ cm, $Q \approx 2\pi$, and $B \approx 5.5$ dB/aperture is capable to provide $N \approx 2000$ resolvable spots at $f_0 \approx 350$ MHz.

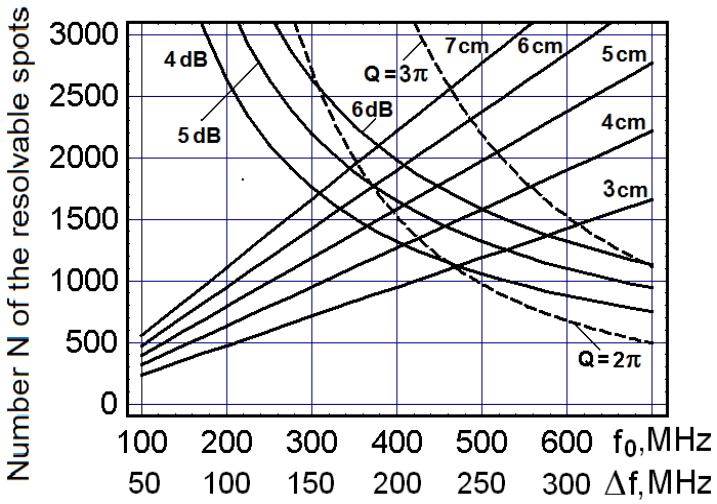

Figure 4. The combined diagram illustrating effect of a triplet of the restricting factors in a gallium phosphide AO cell. The solid slowly growing lines are related to N_1, the chosen apertures D are equal to 3, 4, 5, 6, and 7 cm. The dashed line regards to N_2 in the case of $Q = 2\pi$ and 3π. The solid hyperbolic-like falling curves illustrate N_3 and reflect contributions of the acoustic attenuation; the attenuation factors B are equal to 4, 5, and 6 dB along the aperture.

These estimations have demonstrated that in each considered case the number N of resolvable spots does not exceed the values about 1500 – 2000. With some reasonable restrictions, one can consider these magnitudes as the natural limitation conditioned by various peculiarities of physical processes inherent in the normal regime of light scattering.

4. APODIZATION OF A LIGHT BEAM BY VARIABLE GAUSSIAN PROFILES

At really high acoustic frequencies, the divergence of acoustic beam can be omitted, so that the acoustic attenuation will play the dominating role in the expected asymmetric no-uniformity of distributing the acoustic energy along the AO cell's aperture. Moreover, this asymmetric no-uniformity is not the same within the frequency bandwidth Δf of a cell. The central frequency f_0 is determined as $\Delta f = p\, f_0$. The ratio v of the highest frequency to the lowest one within a given frequency bandwidth is $v = (2 + p)/(2 - p)$. Where p is an experimental value inherent to the characteristics for a specific AO cell, usually $p = 1/2$, and one yields $v = 5/3$. In its turn, the peak-ratio between two amplitude coefficients of the acoustic losses, corresponding to these pair of boundary frequencies within the bandwidth $\Delta f = f_0 / 2$, is $v^2 \approx 2.78$ due to square-low dependence of the acoustic losses on the frequency. Sometimes, however, a little bit wider frequency bandwidth with $p = 2/3$ and $\Delta f = 2\, f_0/3$ is exploited, so that in this case $v = 2$ and, naturally, $v^2 = 4$. Consequently, the expected asymmetric no-uniformity of distributing the acoustic energy cannot be already omitted. To find sufficiently desirable profile of the incident light beam apodization the expected effect of acoustic attenuation has to be estimated. Similar analysis makes it possible to propose exploiting a quasi-Gaussian profile of the incident light beam correlated with the aperture of AO cell with an appreciable acoustic attenuation.

Now, we make an attempt to describe the effect of apodization along an aperture of the AO cell with moderate acoustic losses for the incoming light beam on the potential dynamic range of AO spectrum analyzer. To take into account the contributions from the acoustic losses we shift the origin of the physical coordinate x across a beam so that the magnitude $x = 0$ will be associated with the plane of piezoelectric transducer in an AO cell. In fact, this means that we replace x by $x - 0.5\, D$, where D is the physical cell's aperture measured in centimeters. One can suppose that the electric field amplitude profile $A(x)$, inherent in the issuing beam of a gas laser and reaching the AO cell aperture, is usually close to the Gaussian shape. At this step, let us put $b = 0$, so that one can write (in both real and dimensionless variables) that

$$A(x) = A_0 \exp[-\sigma(x - x_0)^2] = A_0 \exp[-\beta(y - 0.5)^2], \qquad I(y) = |A_0|^2 \exp[-2\beta(y - 0.5)^2]. \quad (2)$$

Here, $y = x / D$ is the normalized dimensionless coordinate along the aperture D, so that $y \in \{0, 1\}$, while σ and $\beta = \sigma D^2$ are physical and dimensionless apodization profile parameters for the Gaussian function.

To realize matching the initial size of laser light beam with the optical aperture of a large-aperture AO cell in the plane of light scattering, i.e. to provide a one-dimensional expanding of the laser beam together with its Gaussian apodization one can exploit a multi-prism beam expander. Such a device can be designed relatively simply and compact using right-angle prisms. With the standard formula for the light refraction [14] by the first facet, i.e. by the border air/glass $\sin \varphi = n \sin \delta$, where n is the refractive index of a glass, one can obtain the factor of beam expanding

$$\text{a)}\ B_1 = \frac{d_1}{d_0} = \frac{\sqrt{(n^2 - \sin^2\varphi)[1 - n^2\sin^2(\alpha - \delta)]}}{n\cos\varphi\cos(\alpha - \delta)}\ , \qquad \text{b)}\ \delta = \arcsin\left(\frac{\sin\varphi}{n}\right), \qquad (3)$$

where α is the top angle of the prism. In the simplest case, when all the glass prisms are identical to each other and the angles φ of incidence are the same for all of them, one can write $B_m = (B_1)^m$ and obtain the needed expanding. Involving, in particular, even number m of the Littrow prisms (i.e. the right-angle prisms 30° - 60° - 90°), the beam direction can be saved with an accuracy of some spatial parallel shift. Equation (3) shows that initially in-phase beam with a Gaussian intensity profile, whose full width can be estimated at a given level (for instance, at a level of e^{-1}), will be expanded by a suitable prism in the same proportion $B_m = d_m / d_0$ on the given intensity level as well due to using an approximation of the geometrical optics, see Fig.5. Then, Eq.(3) determines practically important dependence of B_m and d_m on the angle φ of light incidence on the input facet of a beam expander. The plot describing the linear beam expansion by two sets including $m = \{2, 4\}$ equivalent Littrow prisms with $n = 1.5$ and $\alpha = 30°$ are presented in Fig.6a. It is seen that the corresponding angles φ of incidence become to be rather large for B_m lying in a range of $\{20 - 60\}$.

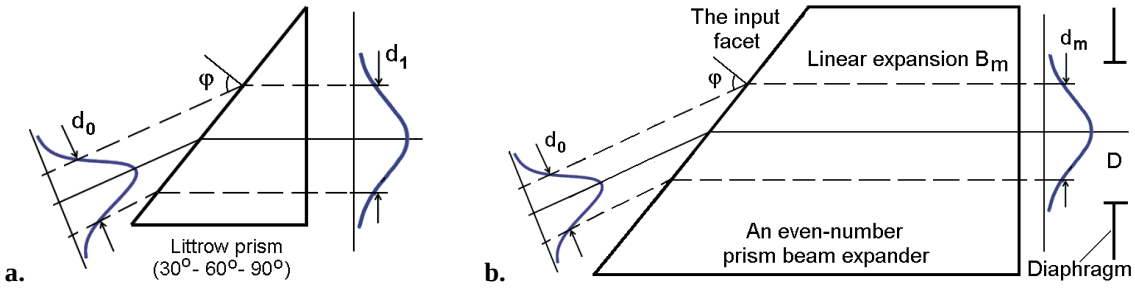

Figure 5. Infinite Gaussian profile passing through a single Littrow prism (a) and an expander with a diaphragm (b).

Let the normalized initial light intensity distribution for Gaussian beam in physical coordinates is characterized by $I_{in} = \exp(-2\,\sigma_0\,x_0^2)$, so that an intensity level of e^{-1} can be reached at $2\,\sigma_0\,x_0^2 = 1$, i.e. at $x_0 = 1/(2\,\sigma_0)^{1/2}$. The full width of this beam at a level of e^{-1} is equal to $d_0 = 2\,x_0 = (2/\sigma_0)^{1/2}$, while $\sigma_0 = 2/d_0^2$. If now this beam will be expanded by $B_m = d_m/d_0$ times, one can write the output light intensity distribution $I_{out} = \exp(-2\,\sigma_m\,x_m^2)$ and then obtain $x_m = B_m\,x_0$, $\sigma_m = 2/d_m^2 = 2/(B_m^2\,d_0^2)$, and $d_m = 2\,x_m = (2/\sigma_m)^{1/2}$. After that one can take into account the diaphragm, whose window is equal to D in physical coordinates, and then introduce the normalized coordinates $y_0 = x_0/d_0$ and $y_m = x_m/D$. In so doing, one yields $I_{in} = \exp(-2\,\beta_0\,y_0^2)$ and $I_{out} = \exp(-2\,\beta_m\,y_m^2)$, where $\beta_0 = \sigma_0\,d_0^2 = 2$ is the input factor and $\beta_m = \sigma_m\,D^2 = 2\,D^2 / d_m^2$ is the apodization factor. One can see that $\beta_m = 2$ with $d_m = D$ providing an intensity level of e^{-1}.Then, one can explain the apodization factor as $\beta_m = 2\,(D^2/d_0^2) \times (d_0^2/d_m^2) = 2\,d^2/B_m^2$, where the ratio $d = D/d_0$ represents the relative output diaphragm. Dependences of the apodization factor β_m on the linear expansion B_m for various magnitudes of the relative output diaphragm d are shown in Fig.6b. It is seen that, when $d^2 = B_m^2$, every time one arrive s naturally at $\beta_m = 2$.

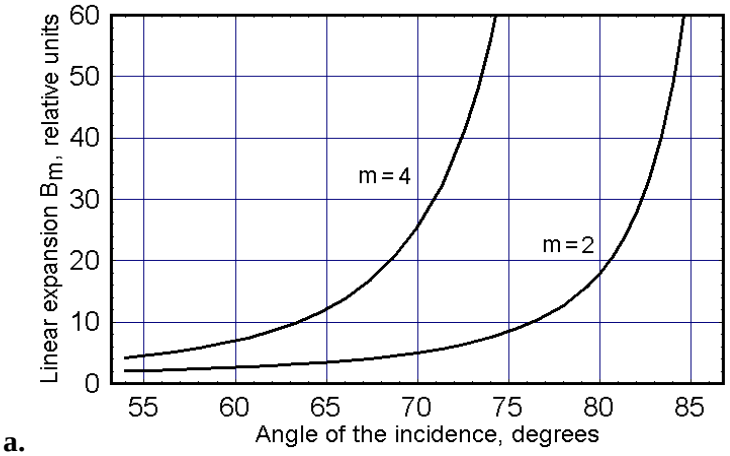

a.

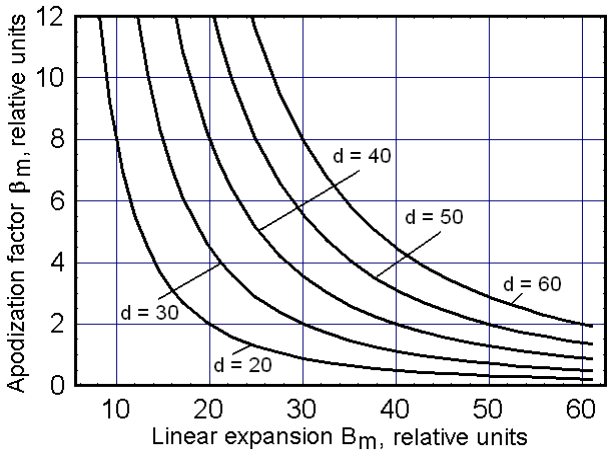

b.

Figure 6.a) Linear expansion B_m providing by two sets of the Littrow prisms with $m = \{2, 4\}$, $n = 1.5$, and $\alpha = 30°$. b) Apodization factor β_m vs. expansion B_m for various relative output diaphragms d.

The illustrating experimental studies on expanding the laser beam with $d_0 \approx 1$ mm and the output diaphragm with $D = 20$ mm, providing the relative output diaphragm $d = D/d_0 \approx 20$, had been carried out using a two-prism beam expander ($m = 2$) with tunable value B_2, i.e. for various magnitudes of the apodization factor $\beta_2 \equiv \beta$. The corresponding traces presenting the light distributions along the fixed window of the output diaphragm, obtained from a 3000 pixel CCD camera (LC1-USB, Thorlabs Inc.) are shown in Fig.7a in absolute units (linear scale; zero level is presented) as well as in the normalized relative units. The corresponding theoretical plots are depicted in Fig.7b.

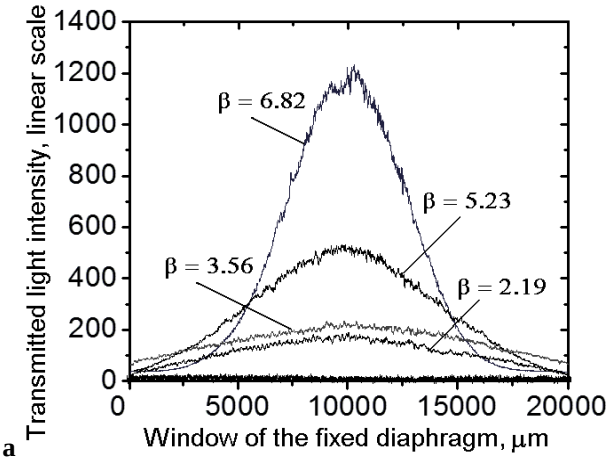

a

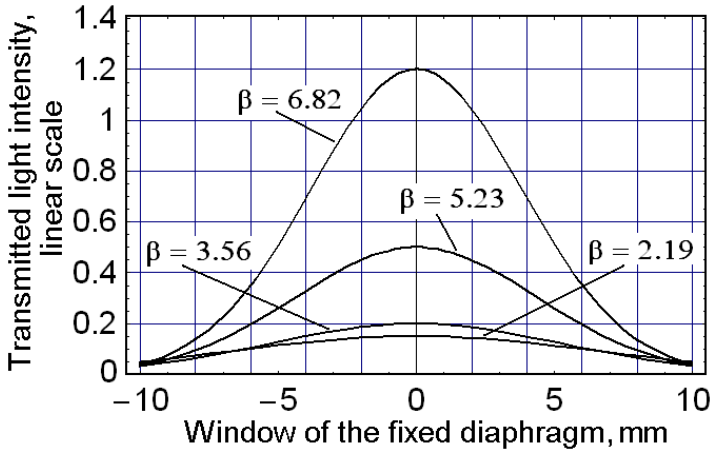

b.

Figure 7. The experimental (a) and theoretical (b) distributions for the transmitted light intensity along the fixed 20 mm-window of the output diaphragm for various magnitudes of the apodization factor $\beta_2 \equiv \beta$:

5. ESTIMATING PERFORMANCES OF THE $LINBO_3$-BASED AO CELL FOR DIRECT ANALYSIS OF ULTRA-HIGH-FREQUENCY RADIO-WAVE SIGNALS

To provide direct spectrum analysis of UHF radio-wave signals the $LiNbO_3$-based AO cell operating in the anomalous light scattering regime with wide-bandwidth tangential phase matching with so-called "optimal matching" can be chosen. As it had been shown in [10], due to taking similar modified geometry of anomalous AO interaction exactly two acoustic wave vectors will intersect the internal optical surface of refractive indices. Therefore, the precise Bragg matching can be fulfilled at a pair of different acoustic frequencies. As a result, close to perfectly symmetric profile of the frequency band-shape will be potentially formed, so that two maxima of a new band-shape will be situated at frequencies almost equidistant from the central tangentially matching frequency. In this case, both the central frequency f_C and the frequency bandwidth Δf_A the for anomalous light scattering are given by [15].

$$\text{a)}\ \ f_C = \frac{V}{\lambda}\sqrt{|n_i^2 - n_d^2|}\,, \qquad \text{b)}\ \ \Delta f_A \approx 2V\sqrt{2n/(\lambda L)}\ , \tag{4}$$

where n is the average refractive index and $L = L_0$ is the initial length of AO interaction. Expression for Δf_A in Eqs.(4) does not include the frequency f_C in the contrast with the corresponding formula for $\Delta f_N \sim 1/ f_C$, leading to fast increasing Δf_N when the central frequency f_C grows.

The above-mentioned approach can be illustrated by the following numerical estimations for a one-fold light scattering in lithium niobate crystalline AO cell operating in the regime of anomalous light scattering with wide-bandwidth tangential phase matching.

The main values N_E and N_O of the refractive indices inherent in a lithium niobate crystal are markedly dispersive; for instance, $N_E \approx 2.208$, $N_O \approx 2.967$ at $\lambda = 633$ nm and $N_E \approx 2.152$, $N_O \approx 2.227$ at $\lambda = 1150$ nm [16], so that their difference i.e. the birefringence has a tendency to fall as the optical wavelength λ grows. This is why choosing the optical wavelength represents a degree of freedom to vary the central frequency f_C, as it is seen from Eqs.(4), in such a way that the frequency f_C can be lowered, for example, to suppress the effect of acoustic losses, via increasing the optical wavelength. In lithium niobate crystal, one can choose the process using the S[100] 35ºY-acoustic mode, so that $V = 3.465\cdot10^5$ cm/s, $n \approx 2.2$ in this case, and select $\lambda = 1150$ nm with $L = 0.2$ cm. Using Eqs.(4), one can calculate $\Delta f_A \geq 300$ MHz and $f_C \approx 1727$ MHz, while $\Delta f_N \approx 13.3$ MHz at the same central frequency f_C and other parameters. For the taken set of material parameters, estimating the Klein-Cook parameter at the minimal frequency in the range, i.e. at $f_{min} = f_C - (\Delta f_A/2) = 1575$ MHz gives $Q = (2\pi/n)\cdot(\lambda L f_{min}^2/V^2) > 1.3\cdot10^3$, which provides the Bragg regime of scattering at f_{min}. The obtained data mean that $\Delta f_A / f_C \approx 17.5\%$, which can be improved, evidently, only through exploiting much more complicated and expansive phased-array technique for arranging the piezoelectric transducer [10].

In this case, N is again limited by the independent agents mentioned previously, but they have to be partially modified because now the above-exploited in section 3 approximation $\Delta f \approx f_0 / 2$ cannot be applied. In so doing, one can use the expression

$$N_1 \le \frac{D}{V} \cdot \Delta f_A \approx 2D\sqrt{\frac{2n}{\lambda L}}, \tag{5}$$

which does not depend on the frequency. The second limitation is not actual now due to the Klein-Cook parameter is high enough even at the minimal frequency in the range of processing. The second limitation is not actual practically due to the carried out above estimation of the Klein-Cook parameter even at the minimal frequency in the range of processing. At the same time, the acoustic attenuation can be extremely important for acoustic waves at the UHF. One can take B ≈ 10 dB/aperture as an acceptable level of acoustic losses along the AO cell's aperture and find an allowable aperture D as

$$D \le B\Gamma^{-1} f_C^{-2} \approx 3.356\, cm, \tag{6}$$

due to $\Gamma \approx 1$ dB / (cm·GHz^2) [17]. However, one has to note here that the information related to the attenuation level for this acoustic mode is rather contradictory, so that the taken value of Γ ought to be considered as a reference one. Substituting Eq.(6) into Eq.(5), one can find

$$N_3 \le \frac{B}{\Gamma V f_C^2} \cdot \Delta f_A \approx 3532. \tag{7}$$

By this it means that one can expect N ≥ 3500 resolvable spots with the $LiNbO_3$-cell under consideration, while the corresponding frequency resolution δf = V / D is close to about 100 KHz.

The efficiency of anomalous AO interaction with wide-bandwidth tangential phase matching in a crystal can be characterized by the modified figure of merit $M_2 = n_0^3 n_e^3 p_{eff}^2 / (\rho V^3)$, where no and ne are the corresponding refractive indices, ρ = 4.7 g/cm^3 is the material density of a lithium niobate crystal, and p_{eff} is the corresponding effective photo-elastic constant. To determine the magnitudes of both p_{eff} and M_2 one can apply the recently developed approach [18] to the case of the slowest shear acoustic wave passing along the [100] -axis in a $LiNbO_3$ -crystal with the displacement vector is oriented along the direction 35º to the [010] -axis. As a result, the maximum value of photo-elastic constant is $| p_{eff,max} | \approx 0.15$, while the maximum for M_2 depends radically on the magnitude of the available refractive indices as well. For the above-chosen case of λ = 1150 nm, one can estimate the AO figure of merit by the value $M_2 \approx 12.7 \cdot 10\text{-}18 s^3/g$ due to $n_0 = n_i = 2.227$, $n_e = n_d = 2.152$, and $V_s = 3.465\ 10\ 5$ cm/s [16]. Figure 8 represents the theoretical band-shape for this $LiNbO_3$-crystalline AO cell, operating in the regime of anomalous light scattering with wide-bandwidth tangential phase matching, calculated using slightly modified design program from [10].

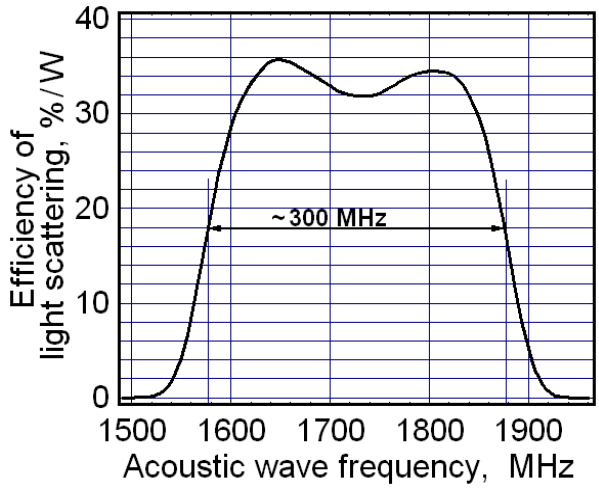

Figure 8. Theoretical band-shape for $LiNbO_3$ AO cell operating in the anomalous regime with wide-bandwidth tangential phase matching.

One can find from this plot that $LiNbO_3$ –based AO cell under discussion is able potentially to provide the efficiency of light scattering up to 36% per one Watt of the applied acoustic power within a 0.405 level of a maximum frequency bandwidth close to 300 MHz.

6. EXPERIMENTAL DATA

Preliminary testing of the optical system, associated with the second spatial arm of a new prototype under consideration, had been preliminary carried out with the currently available (in the meanwhile not optimal) Bragg cell, made of gallium phosphide (GaP) crystal (Molecular Technology GmbH, Berlin), which had an active optical aperture of 50 × 2 mm. Within operating at the dark red optical wavelength of 671 nm (the refractive index $n \approx 3.272$) with linear state of the incident light polarization on the central acoustic frequency $f_0 \approx 380$ MHz, this cell provides the deflection angle of about 1.16 angular degrees and allows a maximum input acoustic power of about 3.0 W. The acoustic wave velocity was estimated by $V \approx 6.3 \times 10^5$cm/s. The experimental studies consisted in two parts. The first one included measuring the bandwidths of AO interaction in the Bragg regime of light scattering in the first order via observation of the frequency bandshape peculiar to that 50-mm aperture GaP crystalline AO cell. The second part of experiments was related to estimating possible resolution of the AO cell via measurements of the light intensity distributions of individual spots in focal plane of the integrating lens for light scattering by the same GaP–cell. The detected frequency band-shape inherent in the wide-aperture GaP–cell exhibits characteristic variations of efficiency at a top of the experimental plot conditioned by some uncoupling of both active and reactive parts of the AO cell's impedance at different acoustic frequencies. Each maximum of efficiency is potentially corresponding to better matching of impedance at the takes radio-wave signal frequency. Practically obtained non-uniformity of the frequency characteristic was equal to about 11%. Total experimental frequency bandwidth at a –3 dB-level had been estimated by the value $\Delta f_{exp} \approx 216$ MHz.

Estimating the frequency resolution peculiar to the GaP–cell within the frames of the above-described optical system (including the CCD-array with 3000 pixels of 7 μm × 200 μm each) had been performed at the wavelength 671 nm as well. Two types of measurements had been realized in the regime of so-called "hot cell", i.e. with a radio-wave signal applied at the electronic input port of that GaP–cell. The first type of measurements had been performed at the almost central acoustic carrier frequency $f_{exp} \approx 380$ MHz with total acoustic wave attenuation $B \approx 4.33$ dB/aperture under action of close to a rectangular, with non-uniformity not more than 10%, incident lighting. Figure 8a depicts the normalized light intensity profile with the spot size slightly exceeding 14 microns and the side lobe level of about 5.1%.

Our experimental results had been obtained using the achromatic integrating lens (Edmund Optics) with $F = 85$ cm at the light wavelength 671 nm, so that theoretically $d_S = \lambda F/D \approx 11.41$ μm with $D = 50$ mm. Together with this, plot in Fig.9a exhibits $d_T \approx 14.12$ due to $\vartheta_T \approx 1.2375$, $m_T \approx 2$, and $D_T \approx 40.4$ mm. The last data show that almost 20**%** of the active optical aperture inherent in the taken GaP crystalline AOC is lost due to imperfectness of both the lens and the AOC's crystalline material. Then, instead of theoretical limit for the frequency resolution $\delta f = V/D \approx 126.4$ kHz, one yields the measured value $\delta f_T = V/D_T \approx 156.4$ kHz. Thus the experimentally obtained number of resolvable spots can be estimated as $N_{exp} = \Delta f_{exp}/\delta f_{exp} \approx 1381$. Finally, the expected lighted area length in focal plane of the integrating lens can be considered as $L_{CE} = d_T N_{exp} \approx 19.5$ mm. This length L_{CE} does not

exceed capabilities of the optical system under consideration based on the CCD-array with 3000 pixels and full lighted area length 21 mm.

The second type of measurements had been carried out using Gaussian apodization of the incident light distribution to demonstrate an opportunity of suppressing side lobes and increasing potential dynamic range of data processing. The chosen profile of the incident lighting was close to the distribution $I_{in} \approx \exp(2\,\beta\,y^2)$ with $\beta \approx 6.0$ and $y = x/D$, where D = 50 mm is active optical aperture of this GaP crystalline AOC and x is the physical coordinate. In this case the acoustic carrier frequency was about $f_{exp} \approx 450$ MHz with total acoustic wave attenuation close to $B \approx 6$ dB/aperture. Figure 9b shows the normalized light intensity profile with the spot size slightly exceeding 21.2 microns with significantly suppressed side lobes, which look as a noise trace at the bottom of this plot**.** The maximum of this profile can be adequately estimated using α_0 = 6 dB at $\beta \approx 6.0$ (compare with the plots in Fig.7.

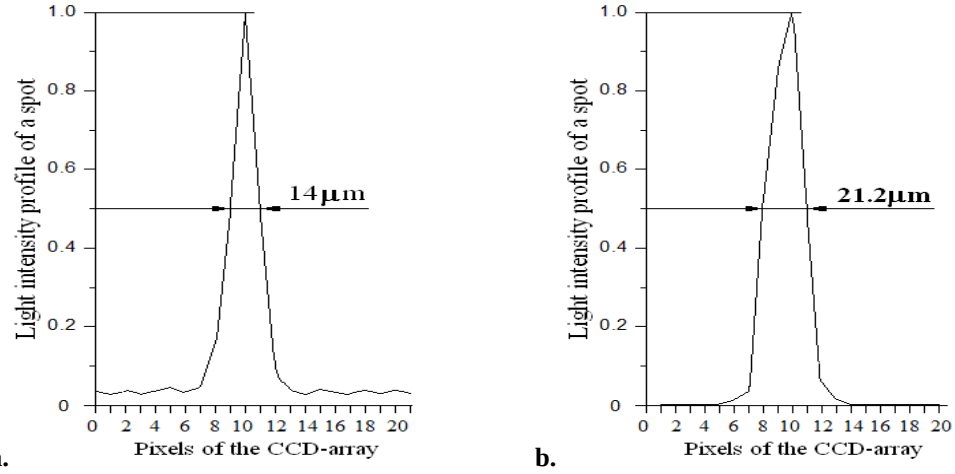

Figure 9. Light intensity profiles of an individual resolvable spot for GaP crystalline AOC with the applied input radio-wave signal at a) $f_{exp} \approx 380$ MHz and b) at $f_{exp} \approx 450$ MHz with Gaussian apodization of the incident light distribution; $\beta \approx 6$.

7. CONCLUSIVE REMARKS

We have developed a pioneer approach to designing a prototype of the radio-wave AO spectrometer that has been confirmed by both the practical estimations and preliminary proof-of-principal experiments. The advances under our proposal reflect the progress in this area consisting in much higher level of parallelism in a wideband analogue data processing with additional frequency performances simultaneously and in exploiting the most appropriate AO materials. We have considered the scheme with a few spatially parallel arms for radio-signal processing, which provide a parallel observation of astrophysical objects within a few different scales simultaneously. Finally, after AO processing, a few data flows are united by the joint matrix CCD photo-detector already on the stage of a high-bit-rate and digital electronic data processing. At the moment, we have restricted ourselves by only three similar spatial arms for radio-wave signal processing.

The first spatial arm represents almost a replica of the optoelectronic scheme described previously [6], so that it need not a lot of additional description. It is based on very effective tellurium dioxide AO cell with the central frequency of analysis about 60 – 80 MHz and the frequency bandwidth below 100 MHz. The second arm is oriented to the spectrum analysis of so-called middle-frequency radio-wave signals with the central frequencies in the range 350 – 500 MHz and the frequency bandwidth about 100 – 300 MHz. This spatial arm exploits currently the AO cells based on gallium phosphide (GaP) single crystal operating in the regime of normal light scattering. The third arm of processing is intended for direct spectrum analysis of UHF radio-signals whose central frequencies lie close to 1.5 GHz and the frequency bandwidth are over 300 MHz. At the moment, the third spatial arm oriented to an AO cell based on rather specific cut of a lithium niobate ($LiNbO_3$) crystal providing the anomalous regime of light scattering in the near infrared optical range. Potentially, one can already have imagined the fourth spatial arm directed to reaching the frequency bandwidths over 1 GHz with the corresponding growth of the central frequencies. Each the enumerated spatial arm for spectrum analysis within the prototype under discussion consists of a few optical or optoelectronic sub-systems.

The three AO cells are key components of the spectrometer under consideration, because just these components determine the efficiency of operation, the frequency bandwidth of spectrum analysis, and the frequency resolution, i.e. the accuracy of radio-wave signals identification. Together with this, even an individual spatially one-channel AO cell provides a multi-channel (a thousand channels or more) parallel processing in the frequency domain in such a way that practical frequency range of AO cell's operation can be varied in wide limits to be perfectly adequate to the observational needs of modern radio-astronomy.

At the current stage of development, our main goals assume the creation and sequential characterization of the enumerated sub-systems for the second arm with the wide-aperture AO cell based the GaP single crystal. During the characterization of the beam shaper, including optical attenuator, linear polarization controller, and a four-prism beam expander, capable of apodizing that beam by the variable Gaussian profile, rather accurate adjusting the incident light beam had been achieved. The processing part of this spatial arm consists of a triplet of the following basic components. The first of them is represented by the

above-mentioned gallium phosphide AO cell (Molecular Technology GmbH) with a 50 × 2 mm active optical aperture. The second component is a fragment of the 3-inch achromatic doublet lens (Edmund Optics) with the focal length of about 85 cm, while the third one is the second row of a multi-row CCD- array consisting of 3000 pixels of 7 μm × 200 μm each. The produced characterization shows that the main lobe of each partial optical beam can give the spot size of about 14-18 μm, so that it is lighting exactly two or three pixels of the CCD-row that guarantees optimal resolution of a pattern from viewpoint of the sampling theorem.

The GaP-cell worked at optical wavelength λ = 671 nm, which combines the convenience of operating in the visible range with good enough transparency of this material with dark red light. This cell was able to manage the radio-wave signals whose the best performances can be estimated as the central frequency ~ 380 MHz, frequency bandwidth is close to 220 MHz and frequency resolution about 150 KHz providing the number $N \approx 2 \times 10^3$ of resolvable spots or, what is the same, the number of parallel frequency channels for spectral data processing.

ACKNOWLEDGEMENTS

We would like to thank CONACyT for financial support through grant CB-256961 and AdlOptics Berlin (Germany)

REFERENCES

1. G. Xia, W. Zheng, Z. Lei, and R. Zhang, "Rigorous coupled wave analysis of acousto-optics with relativistic considerations," J. Opt. Soc. Am. A 32, 1594-1603 (2015).
2. G. Ramírez-Meléndez , M. Bello-Jiménez, C. Cuadrado-Laborde, et al, "Acousto-optic interaction in biconical tapered fibers: shaping of the stopbands", Opt. Eng. 0001;55(3):036105 (2016).
3. A. Grinenko, M. P. MacDonald, C. R. P. Courtney, P. D. Wilcox, C. E. M. Demore, S. Cochran, and B. W. Drinkwater, "Tunable beam shaping with a phased array acousto-optic modulator," Opt. Express 23, 26-32 (2015).
4. J. L. Bertaux et al., "SPICAV on Venus Express: Three spectrometers to study the global structure and composition of the Venus atmosphere", Planetary and Space Science 55 (12) 1673-1700 (2007).
5. M. Dagostino, A. Shcherbakov, A. Arellanes and V. Chavushyan, "High-Resolution Broadband Millimeter-Wave Astrophysical Spectrometer with Triple Product Acousto-Optical Processor," International Journal of Astronomy and Astrophysics, Vol. 3 No. 4, pp. 421-430 (2013).
6. A. S. Shcherbakov and A. Luna Castellanos. "Developing an advanced prototype of the acousto-optical radio-wave spectrometer for studying star formation in the Milky Way", International Journal of Astronomy and Astrophysics. Vol.4, pp.128-144 (2014).
7. I. Peled, R. Kaminsky, and Z. Kotler, "Acousto-optics bandwidth broadening in a Bragg cell based on arbitrary synthesized signal methods," Appl. Opt. 54, 5065-5073 (2015).
8. G. I. Petrov, Z. Meng, and V. V. Yakovlev, "Electronically tunable coherent Raman spectroscopy using acousto-optics tunable filter," Opt. Express 23, 24669-24674 (2015).
9. Z. Meng, G. I. Petrov & V. V. Yakovlev, "Pure electrical, highly-efficient and sidelobe free coherent Raman spectroscopy using acousto-optics tunable filter (AOTF)", Scientific Reports 6, 20017 (2016)

10. A. P. Goutzoulis and D. R. Pape. “Design and fabrication of acousto-optic devices”, Chapter 1. Principles of Acousto-Optics, A. P. Goutzoulis and V. V. Kludzin, pp.1-68. Marcel Dekker, N.Y., 1994.
11. H. Gnewuch, N. K. Zayler, C. N. Pannell et al. “Broadband monolithic AOTF.” Opt. Lett., vol.25, no.5, pp.305-307 (2000).
12. E. Young and S-K. Yao. “Design considerations for acousto-optic devices”. Proc. IEEE, vol.69, no.1, pp.54-64 (1981).
13. A. S. Shcherbakov, A. O. Arellanes Bernabe, and S. A. Nemov. “Transmission function of collinear acousto-optical interaction occurred by acoustic waves of finite amplitude." J. Opt. Soc. Am. – B, vol.30, no.12, pp.3174-3183 (2013).
14. M. Born and E. Wolf. Principles of Optics. 7-d Ed., Chapter 1 (Cambridge University Press, 1999).
15. R. Dixon, "Acoustic diffraction of light in anisotropic media," IEEE Journal of Quantum Electronics, 3 (2), pp. 85-93 (1967).
16. M. P. Shaskolskaya, Handbook of Acoustical Crystals, Nauka Publishers (1988).
17. I. C. Chang, Chapter 12, Acousto-Optic Devices and Applications. In Handbook of Optics. Ed. M.Bass. Vol II. McGrow-Hill (1995).
18. A. S. Shcherbakov, A. O. Arellanes, S. A. Nemov, “Transmission function of the collinear acousto-optical filter controlled by acoustic waves of the finite amplitude”, Opt. Eng. 52(6), 064001 (2013).